Journal of Drug Delivery Science and Technology 81 (2023) 104264

Contents lists available at ScienceDirect

Journal of Drug Delivery Science and Technology

journal homepage: www.elsevier.com/locate/jddst

Polymeric nanoformulation prototype based on a natural extract for the potential treatment of type 2 diabetes mellitus

Elkin Escobar-Chaves [a,b], Sergio Acin [a,d], Diana Lorena Muñoz [d], Maritza Fernández [b], Alexandra Echeverri [a], Fernando Echeverri [c], Jahir Orozco [b], Norman Balcázar [a,d,*]

[a] GENMOL Group, Universidad de Antioquia, Calle 62 # 52-59, Medellin, Colombia
[b] Max Planck Tandem Group in Nanobioengineering, Institute of Chemistry, Faculty of Natural and Exacts Sciences, University of Antioquia. Complejo Ruta N, Calle 67 N° 52–20, Medellín, 050010, Colombia
[c] Group of Organic Chemistry of Natural Product, Faculty of Natural and Exact Sciences, Universidad de Antioquia, Calle 70, N° 52-21, A.A. 1226, Medellin, Colombia
[d] Department of Physiology and Biochemistry, School of Medicine, Universidad de Antioquia, Carrera 51D N° 62-29, Medellin, Colombia

ARTICLE INFO

Keywords:
Polymeric nanocarrier
Obesity
T2DM
Inflammation
Triterpenes
Eucalyptus tereticornis

ABSTRACT

Triterpene-enriched fractions (TFs) from *Eucalyptus tereticornis* demonstrated efficiency when administered intraperitoneally in diet-induced obesity (DIO) mouse model to treat obesity-related type 2 diabetes mellitus (T2DM); however, its oral administration has not yet led to satisfactory results. In this context, we developed a polymeric nanoformulation to transport TFs orally in DIO mice and control obesity and T2DM effects. We encapsulated TFs in a polylactic-co-glycolic acid-based nanocarrier, physicochemically characterized the nanocarriers, and evaluated TFs *in-vitro* release kinetics, *in-vivo* metabolic biomarkers, and released triterpenes in a simulated *in-vitro* human gastrointestinal model. The nanoformulation showed a TFs release of 80% in the first 6h *in-vitro*, and the *in-vivo* assay demonstrated a decrease in mice weight, glycaemia, glucose, and insulin intolerance. Finally, triterpenes released up to 75% in the simulated *in-vitro* human intestine. These results open the way for developing new strategies of therapeutic agents with natural products to control obesity and T2DM.

1. Background

The World Health Organization (WHO) identifies obesity as one of the factors responsible for more than a third of deaths worldwide. Each year, at least 2.6 million adults die due to obesity [1]. Certain diseases are attributable to overweight and obesity; 44% of the world's cases of diabetes, 23% of ischemic heart disease, and 7–41% of cancers, including endometrial, breast, ovarian, prostate, liver, gallbladder, kidney, and colon. Obesity and its main complications, i.e., type 2 diabetes mellitus (T2DM) and cardiovascular disease (CVD), are public health issues, with 60–90% of the reported cases of T2DM being related to obesity [1,2]. The prevalence of diabetes is increasing among all ages worldwide, primarily due to increases in overweight and obesity, unhealthy diet, and physical inactivity. The international diabetes federation reports that 537 million adults worldwide currently have diabetes, so it is necessary to take action and control the advance of this disease; otherwise, 783 million people will have diabetes by 2045 [3].

Currently, therapeutic strategies for obesity and T2DM include hypocaloric diets, physical activity, and pharmacological treatment, like oral chemical hypoglycemic drugs and insulin administration [3]. The presence of collateral effects [2,4], a limited therapeutic effect [5], and the route of administration stimulates the search for new and better therapeutic agents [6]. Plants constitute a valuable source in developing new medications, with the advantage of information about their safety and therapeutic effect *in-vivo*, [7,8]. Approximately 50% of the drugs approved by the Food and Drug Administration (FDA) are plant-derived compounds or their derivatives [9].

Previous studies have identified that a TF; ursolic acid (UA), oleanolic acid (OA), and ursolic acid lactone (UAL), obtained from *Eucalyptus tereticornis* leaves and named OBE100 [10–12], systemically reverse some of the metabolic abnormalities present in Diet-induced obesity (DIO) animal model. Intraperitoneally administrated at 300 mg/kg, it reduces fasting hyperglycemia, glucose and insulin intolerance, total cholesterol, low-density lipoprotein (LDL), and very-low-density lipoprotein (VLDL) levels, blood leptin level and significantly reduces weight of the obese animals [13,14]. Nevertheless, oral administration of the TFs dissolved in PBS does not show any effectiveness (data not published), probably because natural pentacyclic

* Corresponding author. GENMOL Group, Universidad de Antioquia, Calle 62 # 52-59, Medellin, Colombia.
E-mail address: norman.balcazar@udea.edu.co (N. Balcázar).

https://doi.org/10.1016/j.jddst.2023.104264
Received 21 September 2022; Received in revised form 3 February 2023; Accepted 9 February 2023
Available online 10 February 2023

triterpenes have poor water solubility and low oral bioavailability [15].

The oral route is the most common and convenient method for administering medications and nutraceuticals [16]. However, this route often results in drug principle degradation due to the stomach's highly acidic environment and digestive enzymes before entering the systemic circulation [17]. Compounds encapsulated into polymeric nanocarriers are a promising alternative to increase bioavailability [18], facilitating passage through the gastrointestinal tract and reaching the circulatory system without losing activity [17]. Thus, they generate a plausible alternative to the delivery of pharmacologically active compounds to treat several diseases [18]. Different strategies have been studied to encapsulate natural products and bioactive phytocompunds [19] to treat obesity, diabetes, and their associated complications, improving their poor solubility, bioavailability, and stability [20–22]. Examples are chitosan for scutellarine [23], solid lipid nanoparticles of myricitrin [24], nanoemulsions for tea polyphenols [25], and polymeric nanocarriers for curcumin [26].

We aimed to develop an oral nanoformulation that enhanced the promising effect of the OBE 100 fraction, guaranteeing higher stability and bioavailability of the pharmacologically active components present in the natural extract through the oral route. Our particular interest is to demonstrate that oral administration of the OBE100-based nanoformulation has the same effect as intraperitoneal administration. In this study, nanoparticles were developed using poly (lactic-co-glycolic acid (PLGA) as a polymer, which is biocompatible, biodegradable, and stable under physiological conditions and has been shown to protect the compounds loaded inside them from degradation and to favor their sustained release [27]. PLGA is easily internalized into the cell by pinocytosis and endocytosis and is then spontaneously hydrolyzed, producing lactic and glycolic acid quickly metabolized to CO_2 and water via the Krebs cycle [28].

The nanoformulation decreased the body and liver weight, reduced blood glucose, neutral lipid accumulation, and the expression levels of gluconeogenic and lipogenic genes. Moreover, an *in-vitro* simulator of the human intestinal tract showed a triterpene released up to 75%, suggesting that this nanoformulation may have potential use in future human trials. These results contribute to developing a new strategy using natural products as a therapeutic agent combined with nanobiotechnology to control obesity and T2DM.

2. Material and methods

2.1. Chemicals and reagents

Poly (lactic acid-co-glycolic acid) (PLGA); LA: GA 50:50 (RG 503H) (Evonik Industries AG, Essen, Germany); poloxamer 188 (CAS 9003-11-6, Kolliphor®), D-α-tocopherol polyethylene glycol 1000 succinates (vitamin E-TPGS, CAS 9002-96-4), ethyl acetate (CAS 141-78-6), ethanol (CAS 64-17-5), acetonitrile (CAS 75-05-8), sodium dodecyl sulphate (CAS 151-21-3), acetic acid (CAS 64-19-7), dichloromethane (DCM) (CAS 75-09-2) (Sigma-Aldrich, St. Louis, MO, USA) were used to prepare the nanoparticles (NPs).

2.2. Encapsulation of OBE100

Preparation of OBE100 from *Eucalyptus tereticornis* leaves was achieved and characterized following the protocol previously described [10,11]. Briefly, Approximately 25 kg of Eucalyptus leaves were extracted with 96% ethanol, and the crude extract (OBE100) was extracted by liquid-liquid separation with hexane:methanol: water 4:3:1; the organic phase was then collected and filtered under vacuum. Chromatographic profiles were monitored in Gilson® HPLC at a flow rate of 1 ml/min; XDB C18 reverse column, 5 μm 4.6 × 150 mm; mobile phase methanol: water 88:12 (acidified with acetic acid 0.05%); wavelengths 206, 254 and 300 nm; run time 30 min.

Nanoparticles (NPs) were assembled following the emulsion/solvent evaporation method. In brief, 80 mg of PLGA, 80 mg of Kolliphor® P188, 16 mg of OBE100, and 8 mg of D-α-tocopherol were dissolved in 5 ml ethyl acetate and 8 ml of water, vortexed at 3.200 rpm for 20 s, and ultrasonicated at 20% amplitude pulses (Ultrasonicator Q500, Qsonica, Newton, CT, United States). The nanoemulsion was concentrated under 300 bars at 150 rpm for 10 min and 40 °C (Rotavapor® R-300, Buchi, Germany). The resulting polymeric nanoformulation (PNF), OBE100-loaded NPs, and empty NPs; were purified by dialysis (MWCO 12-14 KDa membranes, Spectrum™, Labs, Rancho Dominguez, CA, USA), dissolved in ultrapure water, and lyophilized (Labconco®, freezone 12. 7522800).

2.3. Physicochemical characterization of nanoparticles

The NP size and dispersity (Đ) were characterized by dynamic light scattering (DLS) and the surface charge (ζ-potential) by electrophoretic light scattering (ELS) in a Zetasizer-Pro (Malvern Instruments, United Kingdom) at 25 °C. Transmission electron microscopy (TEM) was used, adding 5 μl of PNF aqueous dispersion (1,5 mg/ml) in a copper grid with a carbon membrane and allowed to dry at room temperature for 24h in a desiccant silica gel chamber. The sample was dyed with uranyl acetate 1% for 8min, washed with deionized water, and observed under the electron microscope Tecnai F20 super Twin TMP microscope (FEI Company, Hillsboro, OR, USA). Thermal analysis was performed by differential scanning calorimetry (DSC) using a TA Instrument Q100 model (New Castle, DE, USA). In brief, 3–17 mg of lyophilized OBE100-loaded NPs, and empty NPs, were sealed in a hermetic aluminium capsule and analyzed at temperatures from 20 to 350 °C at 10 °C/min in a UHP nitrogen atmosphere to obtain the thermograms. Fourier transform infrared spectroscopy (FT-IR) (PerkinElmer, Waltham, MA, USA) was used to analyze the samples. The samples were prepared as potassium bromide (KBr) pellets and measured using 18 scans with a resolution of 4 cm^{-1} at 22 °C. Spectra were collected from 4.000 to 450 cm^{-1} wavenumbers.

2.4. Determination of encapsulation efficiency, extract-loading capacity, and release kinetics of triterpenes-rich fraction (OBE100)

Two mg purified and lyophilized OBE100-loaded NPs were diluted in 500 μl of absolute methanol and 500 μl of acetonitrile 95%, sonicated for 20 min at 45 °C to ensure the rupture of the NPs and centrifuged at 14.000 rpm for 20 min The supernatant was filtered, and the amount of extract released was determined by HPLC [11]. The extent of loading capacity (% LC) and encapsulation efficiency (% EE) was determined from the following equations:

$$\%\,\text{Encapsulation Efficiency}\,(\%EE) = \left(\frac{Wt}{Wi}\right) \text{x } 100 \quad \%\,\text{Loading Capacity}\,(\%LC) = \left(\frac{Wt}{Wn}\right) \text{x } 100$$

where (*Wt*) means the amount of encapsulated triterpenes, (*Wi*) the amount of extract initially added to nanoformulation and (*Wn*) the total quantity of excipients used in the preparation.

The sample and separate (SS) method [29] was used to evaluate release kinetics. Twelve mg lyophilized OBE100-loaded NPs were diluted in 3 ml of phosphate buffer pH 7 or 3 ml of citrate buffer pH 3 or pH 5 and incubated until 72 h at 37 °C with intense shaking. Samples at 2, 4, 6, 24, 48 and 72 h were taken and centrifuged for 30 min at 10.000 rpm. The supernatant was filtered and stored for HPLC's analysis and quantification of the release profile.

2.5. Glucose and insulin tolerance test in a diet-induced obesity mouse model

In vivo metabolic activities were evaluated in a diet-induced obesity

mouse model (DIO). C57BL6/J male mice (Charles Rivers Laboratories, Wilmington, MA, USA) four to five weeks old were used. Mice were housed at 22 ± 2 °C with a 12:12 h light-dark cycle with free access to food and water. Mice were randomly divided into six groups for this study (6–8 mice in each group). A control group was fed a normal diet (Chow:14% fat, 54% carbohydrates, and 32% protein). The other five groups were fed a high-fat diet for 12 weeks (HFD: with 45% fat, 41.2% carbohydrates, and 20.8% protein) (DIO Rodent Purified Diet W 45% Energy Fat - 55629, TestDiet, St Louis, MO, USA). Currently, mice are obese and have insulin resistance. HFD + (IP300) and HFD + (IP214) received intraperitoneal (IP) injections of 300 and 214 mg/kg b.w of OBE100, respectively. HFD + (NP) and HFD + (NP214) receive empty NP and 214 mg/kg OBE100-loaded NP orally in a fed state, respectively. Chow and HFD control groups were orally administrated with PBS. All animals received 15 doses every day after. The IP300 is the treatment control group. In the nanoformulation, 214 mg/kg OBE100 was used in loaded NP because it is the amount in 300ul of the solution, and this is the maximum amount allowed to be orally administrated to the mouse. In order to evaluate the biological effect of the same amount of OBE100 administered by different routes, 214 mg/kg was administered intraperitoneally.

An intraperitoneal glucose tolerance test (IPGTT) and insulin tolerance test (ITT) were measured before and after treatments, as described previously [18]. Homeostasis model assessment (HOMA) of insulin resistance (HOMA-IR) was calculated as (fasting glucose level X fasting insulin level/22.5 × 18). Finally, mice were sacrificed, and blood, liver, and adipose tissue were collected for further analyses. All animal studies were approved by the Institutional animal care and use committee of the University of Antioquia (Protocol number 65).

2.6. Serum biochemical parameters

Plasma glucose level was measured using a glucose oxidase-peroxidase kit (BioSystems, Bogotá DC, Colombia); Plasma insulin level was measured using an enzyme-linked immunosorbent assay (ELISA) kit (Mercodia AB, Uppsala, Sweden). Total cholesterol (TC, 11505), plasma total triacylglycerol (TAG, 11528), low-density lipoprotein cholesterol (LDL, 11585), high-density lipoprotein cholesterol (HDL, 11523), alanine aminotransferase (11832), aspartate aminotransferase (23531) (BioSystems), Leptin (ab100718) was quantified by ELISA kit (Abcam, Cambridge, United Kingdom). All determinations were done following the manufacturer's recommendation, and the absorbance was measured using a VarioskanTM LUX multimode microplate reader (Thermo- Fisher Scientific).

2.7. Histological, neutral fat detection, and immunohistochemical determinations

After treatments, mice were sacrificed, and a sample of the livers and visceral adipose tissue was stored in neutral formaldehyde and embedded in paraffin wax. Hepatic fat content was evaluated with the Oil Red-O stain kit ($C_{26}H_{24}N_4O$, ab150678, Abcam, US). Fresh or frozen tissue sections in OCT of 10–12 μm were mounted on electrocharged slides, 500 μl of oil red solution were added and incubated at room temperature for 10 min, then washed and scanned images were obtained at 20X by VENTANA DP 200 slide scanner (Roche, Rotkreuz, Switzerland) and quantified in ImageJ software (NIH).

For immunohistochemical determinations, sections of 6–7 μm from wax blocks were stained on electrocharged slides. The sample was deparaffinized, incubated in H_2O_2 solution 6% for 5 min, and washed with TBST (Tris-buffered saline with tween 20) 1X. Antigen retrieval and staining were performed by adding the primary antibody diluted Acetyl-CoA carboxylase (ACC) (1/200), pACC (1/800), AMP-activated protein kinase (AMPK) (1/500), and pAMPK (1/300) for liver samples and Uncoupling protein one (UCP-1) (1/200) for adipose tissue, for 1 h in the chamber wet. To stain, 100 μl of the 3,3 diaminobenzidine (DAB) Quanto chromogen solution was added with the DAB Quanto substrate (Vitro SA master diagnostica®, Sevilla, Spain) and counterstained with hematoxylin. Scanned images were obtained at 20X by VENTANA DP 200 slide scanner and quantified in ImageJ software (NIH). Five animals per group were analyzed.

2.8. RNA extraction and real-time PCR

After sacrifice, livers and visceral adipose tissues were immediately frozen in liquid nitrogen. Total RNA was extracted from liver and visceral white adipose tissue with a Direct-zol RNA Miniprep kit (Zymo Research) and quantified in nanodrop (Thermo-scientific). The reverse transcription reaction was performed with 500 ng of total RNA, 50 ng/μl of random hexamers, 100 mM dNTP Mix, 10X Buffer, 40 U/l of RNaseOut, and 200 U/l of SuperScript III RT (Invitrogen, Waltham, MA, USA), according to the manufacturer's instructions. Real-time quantitative PCR (qPCR) analyses were performed with 50 ng cDNA and 100 nM sense and antisense primers (Integrated DNA Technologies, Coralville, IA, USA) in a final reaction volume of 25 μl by using the Maxima SYBR Green/ROXqPCR Master mix (Thermo-Scientific) and the CFX96 real-time PCR detection system (Bio-Rad). The thermal cycling program was 10 min at 95 °C, followed by 40 cycles of 15s at 95 °C, 30s at 60 °C, and 30s at 72 °C. The results were normalized to cyclophilin expression levels using the comparative Ct method. Specific primer sequences are provided in supporting information in Table S2.

2.9. Triterpenes release profile in an in-vitro system simulating the human gastrointestinal tract

The Human Intestinal Microbial Ecosystem (SHIME®) simulator is a scientifically validated tool to evaluate the behaviour of foods, nutraceuticals and probiotics as they pass through the gastrointestinal tract [30,31]. This study modified SHIME to evaluate the triterpene release from NPs without microbiome inoculation. The conditions and culture media components used in each reactor follow the indications described in Table S1. After completion of the residence time in each reactor, a sample of 2 ml was acidified with 80 μl of acetic acid and centrifugated 3000 *g* for 10 min; the supernatant was added with 12 ml of DCM-ethyl acetate and vortex mixed for 3min and the organic phase was evaporated and concentrated in a Savant SpeedVac vacuum (Thermofisher, scientific) 45 °C for 45min. The material was resuspended in 1 ml of methanol, filtered in a 0,22 μm filter and quantified using HPLC.

2.10. Statistical analysis

Data are presented as means ± SEM. Comparisons between groups were analyzed using a one-way analysis of variance (ANOVA) followed by a Dunnett post hoc test. Student's t-tests were used for individual pairwise comparisons of least square means. The trapezoidal rule determined the area under the curve (AUC). Differences were considered significant at $P < 0.05$. Analyses were performed with the Prism 8 (GraphPad Software Inc., La Jolla, CA, USA) statistical software.

3. Results

3.1. Preparation and physicochemical characterization of polymeric nanoformulation

Polymeric nanoformulation (PNF) was successfully developed and physicochemical characterized by estimating size and Đ by DLS (Fig. 1C), showing the media size of OBE100 loaded NPs of 168 nm ± 0.01 (Đ of 0.19 ± 0.02) compared with empty NPs of 150 nm ± 0.02 (Đ of 0.14 ± 0.01) and confirmed by TEM morphology image, observing spherical and irregular border NPs as we expected (Fig. 1B). Furthermore, the ζ-potential from Fig. 1C shows that the mean surface charge of OBE100-loaded NP is −38 mV and decreased compared with −43 mV of

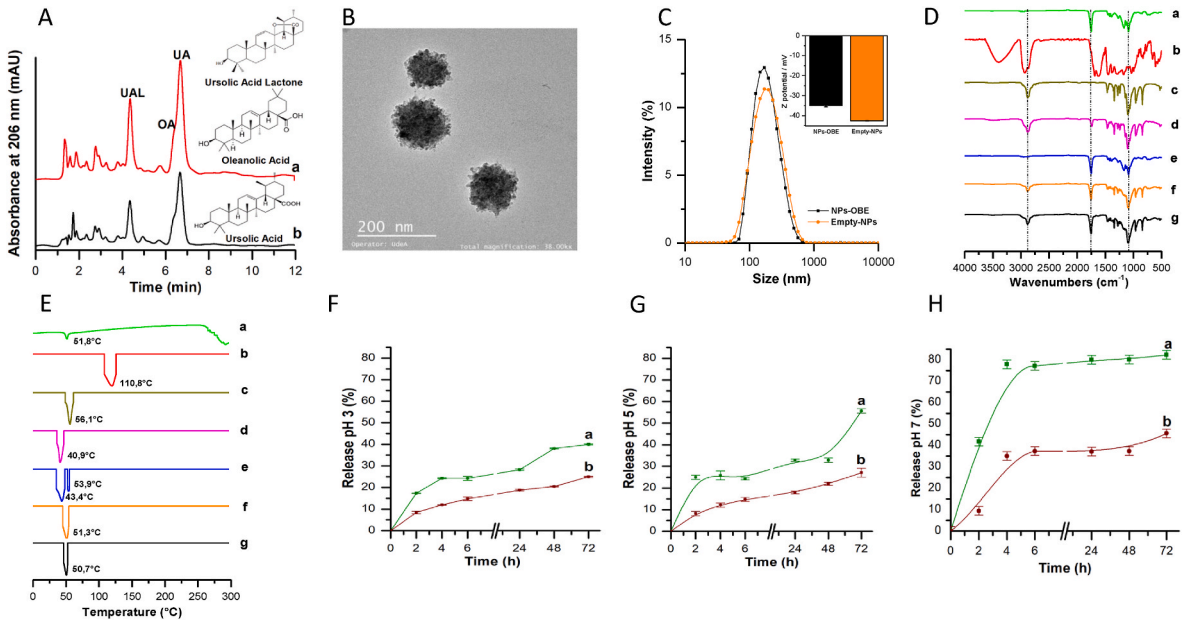

Fig. 1. Physicochemical characterization and release profile for polymeric nanoformulation. (A) chromatographic profiles, OBE100 before (a) and after release from the NPs (b). (B) Morphologic characterization by TEM. (C) Hydrodynamic size and ζ-potential of OBE100-loaded NP (black) and empty NP (Orange). (D) Spectra of PNF and their precursor components by FT-IR and (E) DSC; PLGA 50:50 (a), OBE100 (b), kolliphor P188 (c), D-α-tocopherol (d), physical mixture of precursors (e), OBE100-loaded NPs (f) and empty NP (g). (F) the release profile for OBE100-loaded NP; main triterpenes UAL (a) and OA + UO mix (b) in sink conditions buffer pH3, (G) pH5, and (H) pH7. n = 3. (For interpretation of the references to colour in this figure legend, the reader is referred to the Web version of this article.)

empty NPs. However, these values indicate that NPs are electrostatically stable and have a low aggregation tendency.

FT-IR (Fig. 1D) and DSC (Fig. 1E) were performed to characterize the nanoencapsulation process and determine OBE100-PLGA and precursors components interactions. Fig. 1D shows the FT-IR spectra of the individual precursors (a–d), the physical mixture (e), empty (f) and OBE100-loaded NPs (g). The physical mixture shows signals mainly from the contribution of peaks at 1752 cm^{-1} (C═O stretching) of PLGA 50:50, a small peak at 1643 cm^{-1} (C═O stretching), and at 2882 cm^{-1} (C═O stretching), and 1104 cm^{-1} (C–O stretching) of the two stabilizing surfactants. The physical mixing pattern changed in the OBE100-loaded NPs (g) concerning empty NPs (f), showing a peak at 1767 cm^{-1} (C═O stretching) of higher intensity. The characteristic peaks of OBE100 at 3500 - 3000 cm^{-1} (C–H), 1750 cm^{-1} (C═O stretching) related to δ lactones, and 1232 cm^{-1} (C–N stretching) cannot be observed in PNF OBE100-loaded, indicating PLGA-OBE100 interactions.

Fig. 1E shows the DSC analysis of the individual precursors (a-d), the physical mixture (e), and empty (f) and OBE100-loaded PNF (g). Thermograms show the glass transition temperature and single endothermic melting peak at 51.8 °C, 56.1 °C, and 40.9 °C of 50:50 PLGA polymer (a), kolliphor P188 (c), and tocopherol (d) surfactants, respectively. In addition, two temperature transitions were observed at 43.4 °C and 53.9 °C for the components' physical mixture, which correlates well with those observed for kolliphor P188 (c) and tocopherol (d). In comparison, free OBE100 (b) shows a single endothermic melting peak at 110.8 °C, while empty NPs (f) show the same peak at 51.3 °C. Surprisingly, the free OBE100 melting peak wholly disappeared in the PNF OBE100-loaded thermogram (g), suggesting that PLGA and OBE100 may have a chemical interaction of triterpene functional groups with carboxyl groups of the hydrophobic and hydrophilic tails of PLGA.

3.2. Encapsulation efficiency, extract-loading capacity, and in-vitro release kinetics of OBE100

OBE100-loaded NPs were fragmented, and their chromatographic profile was compared with the profile before encapsulation (Fig. 1A). As a result, the encapsulation efficiency was 92%, and the loading capacity was 6.4%. Therefore, this nanoformulation is highly efficient in encapsulating hydrophobic pentacyclic triterpenes.

UAL and OA + UA release kinetics from the NPs were evaluated in a release medium containing 3% w/v SDS to ensure sink dilution conditions and emulate physiological parameters *in-vitro* for stomach and intestine in mice [32] and humans, with pH3 (Fig. 1F) and pH5 (Fig. 1G) at 37 °C and PBS pH7 (Fig. 1H) at 37 °C. Results show that 25% UAL was released in the pH3 and pH5 citrate acid buffer during the first 6h but progressively increased to 40 and 55% in 72h. We observed a similar tendency in the release profile of the OA + UA mixture, with 15% release in the first 6h that increased to 23% in 72h. In contrast, in buffer pH7, OBE100-loaded NP released 76% UAL and 37% OA + UA mixture in the first 6h and up to 80 and 40%, respectively, in 72h. These results suggest that main triterpenes in neutral conditions have a higher release profile than in acidic conditions, making the PNF suitable for slightly releasing these molecules into the stomach but enhancing the release into the small intestine of mice and humans. Furthermore, it suggests they may be available for absorption, improving their solubility and bioavailability.

3.3. In-vitro releases kinetics of OBE100 on simulated in-vitro human gastrointestinal conditions

To approximate how OBE100 and its main triterpenes are released under simulated conditions of the human gastrointestinal tract, we used the in-vitro SHIME® model without microbiota addition. OA + UA mixture was released up to 91%, i.e., 39, 29, 17 and 6% throughout the system in the stomach, small intestine, ascending colon, and transverse colon at 3,7,27, and 59h, respectively (Table 2). OBE100-loaded NPs released up to 82% of UAL after 27h of system residence: 63% in the stomach, 11% in the small intestine, and 8% in the ascending colon at 3,7, and 27h, respectively (Table 2). UAL was not detected after this time with the analytical method used.

3.4. Polymeric nanoformulation reduces body weight and improves carbohydrate metabolism in the DIO mouse model

Treatment with NP214 reduced 10% of the mice's body weight compared with HFD and NPs mice. A similar body weight reduction (12%) was shown by treatment with the same OBE100 dose administered intraperitoneally (Fig. 2A and B). A higher weight change (18%) was observed when mice were treated intraperitoneally with a dose of 300 mg/kg, used as a positive control. These results suggest that OBE100 modulates body weight reduction regardless of the route of administration.

IPGTT and ITT tests were conducted to determine mice's glucose tolerance and insulin resistance. The results were analyzed as the total area under the curve (AUC) between 0 and 120 min or 0 and 60 min, respectively. IPGTT and ITT showed decreased glucose tolerance and insulin resistance in mice with diet-induced obesity (HFD) compared with the control group (standard chow). When treated with OBE100 (NP214, IP214 and IP300), glucose intolerance and insulin resistance were reverted in obese mice (HDF), showing that oral administration is as effective as intraperitoneal administration (Fig. 2C–F). Mainly, the ITT test showed that NP214 treatment reduced 24.2% in the first 15 min compared to 8% of glucose levels observed after empty NPs treatment. These results suggest that unloaded NPs do not significantly affect carbohydrate metabolism (Fig. 2F and G).

HOMA-IR values were increased in HFD and NPs groups but decreased significantly in all groups treated with OBE100 (Fig. 2H). The HFD group showed an elevated fasting blood glucose level (191.3 mg/dl) (Table 1). However, after treatment with NP214, IP214 or IP300, fasting blood glucose levels were reduced to 156.6, 139.6 and 114.9 mg/dl, respectively (Table 1). Obese mice also exhibited elevated fasting blood insulin levels (7.1 mU/L). The mice's blood insulin levels were significantly reduced when they were treated with OBE100, regardless of the administration route (Table 1). These results suggest that oral OBE100 NPs reduce fasting hyperglycemia, glucose intolerance, insulin resistance, and improved insulin sensitivity in pre-diabetic mice.

3.5. Polymeric nanoformulation improves serum parameters in the DIO mouse model

HFD mice group increased their body weight by 37% compared to the standard chow group after ten weeks and was associated with increased plasma total cholesterol (TC), triacylglycerol (TAG), LDL, and HDL levels (Table 1). All OBE100 treatments significantly reduced mice body weight (Fig. 2A), TAG and LDL levels, but only intraperitoneal administration of OBE100 significantly reduced TC levels (Table 1). Notably, NP214 reduced TAG by 30% and LDL by 38% compared to the HFD group. Although a trend in total cholesterol reduction was observed (13%), this reduction was not statistically significant compared to HFD (Table 1). HDL levels were also reduced by IP300 and IP214 treatments. Surprisingly, NP214 increased HDL levels which may explain the non-significant TC reduction in this group (Table 1). Serum leptin levels increased significantly in the HFD group compared to standard chow. IP300 and IP214 treatments significantly reduced leptin levels by 91 and 67%, respectively, but NP214 had no effect (Table 1). HFD increased Aspartate transaminase (AST) and Alanine transaminase (ALT) levels significantly by 33 and 83%, respectively, compared to the standard chow group. All treatments significantly reduced AST and ALT levels after 15 doses. These results demonstrate that OBE100 and its main triterpenes encapsulated in oral polymeric NPs improve plasma lipid levels.

3.6. Polymeric nanoformulation improves liver markers in the DIO mouse model

HFD feeding is associated with hepatic steatosis [33]. Liver weights increased significantly in mice fed an HFD compared to those fed a standard chow diet. Mice treated with IP300, IP214, and NP214 reduced liver weight compared with the HFD group, while treatment with empty NP did not affect liver weight (Fig. 3B). These results are consistent with liver fat accumulation. HFD-fed mice significantly increased lipid accumulation inside hepatocytes, and only IP300, IP214, and NP214 treatments reduced fat content (Fig. 3A and C). A quantitative evaluation of immunohistochemical staining using antibodies to ACC, pACC, AMPK, and pAMPK (Fig. 3A) showed increased protein expression in

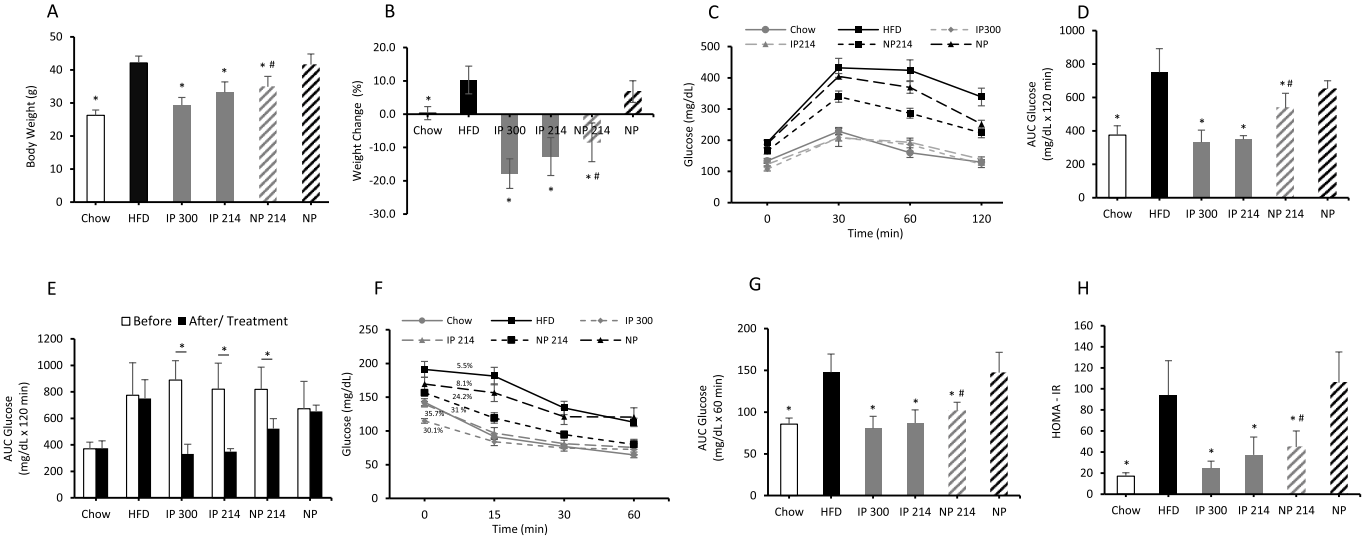

Fig. 2. PNF effect in the assessment of animal weight and carbohydrate metabolism. (A) body weight and (B) weight change in pre-diabetic mice treated intraperitoneally with doses of 300 mg/kg (IP300) and 214 mg/kg (IP214) of OBE100; 214 mg/kg of OBE100-loaded NP (NP214) and empty NP (NP) orally. (C) Glucose tolerance tests (IPGTT) and (F) Insulin tolerance test (ITT) after treatment. (D and G) the AUC for glucose and insulin, calculated from the data obtained in (C and F), respectively, and (E) AUC glucose before/after treatments. (H) Homeostasis model assessment of insulin resistance (HOMA-IR) in pre-diabetic animals with the different treatments. HFD: High Fat Diet. (n = 6–8 mice/group). Values were expressed as mean ± standard error. *: $p < 0.05$, all groups vs HFD group. #: $p < 0.05$, NP214 vs NP, ns: non-significant.

Table 1
Serum parameters for the male C57BL/6 mice fed with Chow, High Fat Diet (HFD) and HFD plus treatment.

	Chow	*p	HFD	IP 300	*p	IP 214	*p	NP 214	*p	NP	*p
Insulin (mU/L)	1.7 ± 0.2	*	7.1 ± 2.8	3.0 ± 0.6	*	4.0 ± 1.6	*	4.4 ± 1.8	*, #	9.3 ± 2.9	n.s
Fasting Glucose (mg/dL)	142.6 ± 15.8	*	191.3 ± 31.0	114.9 ± 9.8	*	139.6 ± 10.5	*	156.6 ± 12.7	*	169.4 ± 2.9	n.s
TC (mg/dL)	72.7 ± 10.4	*	263.0 ± 40.8	96.7 ± 14.7	*	124.4 ± 15.1	*	228.3 ± 22.1	n,s	226.3 ± 37.2	n.s
TAG (mg/dL)	90.0 ± 13.5	*	145.4 ± 28.0	96.4 ± 15.6	*	104.6 ± 15.4	*	102.0 ± 18.5	*, #	161.2 ± 46.6	n.s
LDL (mg/dL)	34.8 ± 3.1	*	82.7 ± 7.6	42.4 ± 2.9	*	50.0 ± 7.1	*	51.8 ± 10.1	*, #	63.7 ± 13.5	*
HDL (mg/dL)	49.1 ± 2.7	*	59.3 ± 3.1	44.5 ± 2.0	*	45.3 ± 4.9	*	62.2 ± 3.3	*	59.9 ± 2.9	n.s
Leptin (pg/mL)	188.2 ± 79.4	*	68894 ± 8178.4	5906 ± 2548.9	*	22481 ± 4096	*	60385 ± 6321	n,s	52640 ± 7554	n.s
AST (U/L)	81.8 ± 9.8	*	122.2 ± 31.3	56.8 ± 6.5	*	61.1 ± 14.7	*	70.5 ± 10.9	*	58.2 ± 15.1	*
ALT (U/L)	15.6 ± 11.6	*	93.9 ± 30.6	17.3 ± 5.0	*	20.1 ± 4.3	*	25.0 ± 12.1	*	42.7 ± 27.4	*

TC: total cholesterol. TAG: triacylglycerol; LDL: Low-density lipoprotein; HDL: High-density lipoprotein. HFD: High-fat diet. Intraperitoneal (IP) administration of 300 (IP 300) and 214 (IP 214) mg/kg of OBE100, oral administration of nanoformulation with 214 mg/kg of OBE 100 packed in nanoparticles (NP 214) and nanoparticles alone (NP). The values represent the means ± SD; *: $p < 0.05$, All Groups Vs. HFD Group. #: $p < 0.05$, NP 214 Vs NP. N = 6–8 mice/group. n.s: non-significant.

Table 2
Digestive conditions and triterpenes released assay using in a modified simulator of the Human gastrointestinal Ecosystem (**SHIME**).

Reactor	Description	pH	Residence time (h)	Accumulated Time (h)	Released UAL x reactor (%)	SD	Accumulated UAL Release (%)	Released OA + UA x reactor (%)	SD	Accumulated OA + UA release (%)
1	Stomach	2	3	3	63	0.26	63	39	0.06	39
2	Small Intestine	6.5–7.0	4	7	11	1.86	74	29	0.23	68
3	Ascending colon	5.0–5.5	20	27	8	0.52	82	17	0.30	85
4	Transverse colon	6.0–6.4	32	59	ND	–	–	6	0.23	91
5	Descending colon	6.4–6.8	24	83	ND	–	–	ND	–	–

UAL, Ursolic acid lactone. OA, Oleanolic acid. UA, Ursolic acid. ND, non-detected. SD, the values represent the mean ± SE. Three independent experiments with three replicas each.

HFD mice compared with standard chow. IP300, IP214, and NP214 treatments reduced all protein expression. We detected an expression reduction for ACC, pACC, and pAMPK but not for AMPK in mice treated with empty NPs (Fig. 3D and E). These results suggest that OBE100, regardless of the route of administration, reduces liver weight and hepatic lipid accumulation associated with expression changes in ACC and AMPK.

To verify whether treatments led to changes in gluconeogenic, lipogenic, and lipolytic gene expression, we assessed mRNA levels in the liver using qPCR. Any Treatment with OBE100 led to a significant reduction of the expression of PEPCK and G6PC1 gluconeogenic genes (Fig. 4A and B) and the expression of lipogenic genes such as ACC and FAS (Fig. 4C and D) compared to the HFD group. On the other hand, the expression of lipolytic genes, CPT1A and PAPRA, was reduced by IP300 and IP214 treatments, while NP214 did not significantly modify their expressions (Fig. 4E and F). Interestingly, NPs treatment did not modify the expression of any gene analyzed (Fig. 4). These results suggest that oral administration of OBE100 NPs, similar to IP300 treatment, regulates the expression of gluconeogenic and lipogenic genes.

3.7. Polymeric nanoformulation effect on adipose tissue in DIO mouse model

Visceral fat weight increased significantly in mice fed an HFD compared to those fed the standard chow diet. Mice treated with IP300 and IP214 had significantly reduced visceral weight, while this effect was not observed in mice treated with NP214 or NPs (Fig. 5A and C). These results are consistent with the adipocyte area. IP300 and IP214 treatments significantly decreased adipocyte area in visceral fat tissue (Fig. 5D). Uncoupling protein 1 (UCP-1) is a well-known protein related to thermogenesis and white adipose tissue browning. Immunohistochemical staining was performed to measure UCP-1 expression in visceral adipose tissue (Fig. 5B). Mice treated with IP300 or IP214 treatment had significantly increased UCP-1 expression. This effect was not observed with NP214 or NPs treatments (Fig. 5D and E). We analyzed the expression levels of leptin by qPCR. HDF increased the expression of this gene in visceral adipose tissue (Fig. 5F), according to high serum leptin levels observed (Table 1). The gene expression of leptin was reduced only with the IP treatment compared to the HDF group (Fig. 5F). These results suggest that only the intraperitoneal administration of OBE100 significantly reduces adipose tissue and modulates the expression of UCP-1 and leptin.

4. Discussion

We developed an efficient polymeric NP to encapsulate a raw natural extract of *Eucalyptus tereticornis* and improve the effects of obesity and T2DM on DIO mice by oral administration. In previous studies, the effect of OBE100 as a potential phytotherapeutic for the treatment of obesity and T2DM was demonstrated [10,13]; however, intraperitoneal administration may not be the best option to guarantee treatment adherence. Therefore, with the development of PNF with OBE100 efficiently encapsulated, we increased the stability and oral bioavailability of the active compound and obtained the biological effect in DIO mice.

Apart from the polymer from our nanoformulation, other biocompatible and biodegradable polymers have been used for nanoencapsulation of drugs, tissue engineering, and theragnostic cancer applications [34]. Besides, layered double hydroxide (LDH) nanoparticles have been proposed as a nanocarrier of improved biocompatibility and reduced cytotoxicity [35].

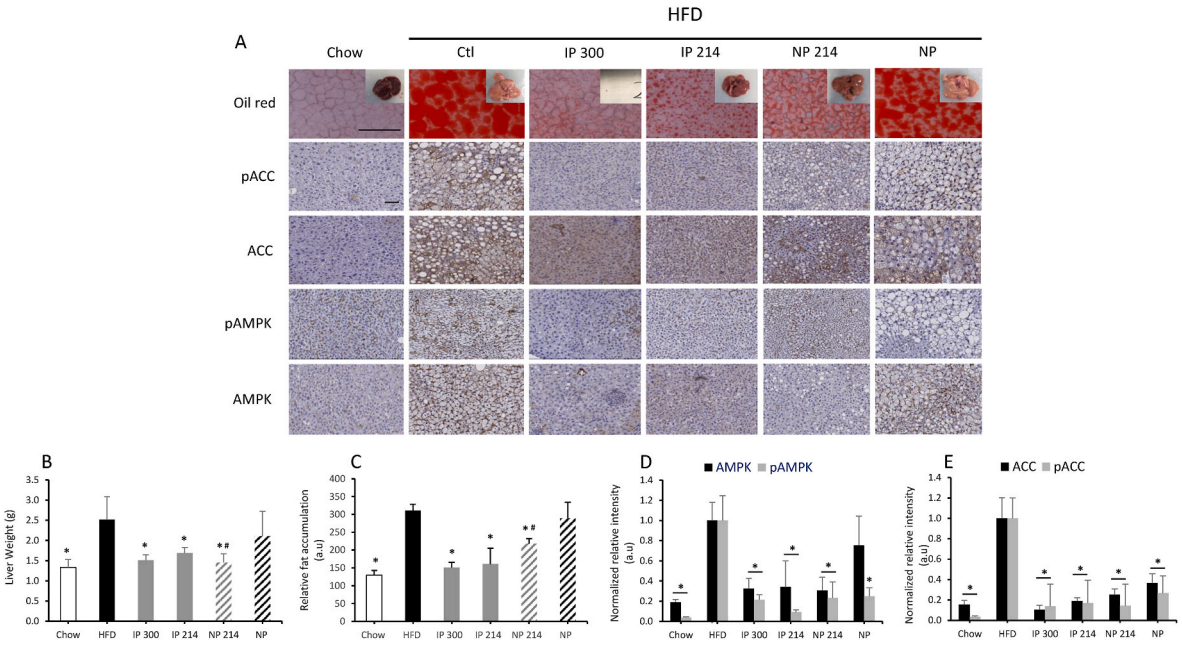

Fig. 3. Effect of PNF treatment on DIO mouse model liver. (A) Liver oil red staining for fatty acids and protein expression immunohistochemistry for phosphorylated acetyl-CoA carboxylase (pACC), acetyl-CoA carboxylase (ACC), phosphorylated AMP-activated protein kinase (pAMPK), and AMP-activated protein kinase (AMPK) in pre-diabetic mice treated intraperitoneally with doses of 300 mg/kg (IP300) and 214 mg/kg (IP 214) of OBE100; 214 mg/kg of OBE100-loaded NP (NP214) and empty NP (NP) orally. (B) Mice's liver weight. (C) Mice's liver tissue area dyed with oil red. Immunohistochemical normalized to cell number for (D) ACC, (E) pACC, (F) AMPK, and (G) pAMPK. HFD: High Fat Diet. (n = 6–8 mice/group). Values were expressed as mean ± standard error. *: $p < 0.05$, all groups vs HFD group. #: $p < 0.05$, NP214 vs NP, ns: non-significant. Scale bar = 100 μm. (For interpretation of the references to colour in this figure legend, the reader is referred to the Web version of this article.)

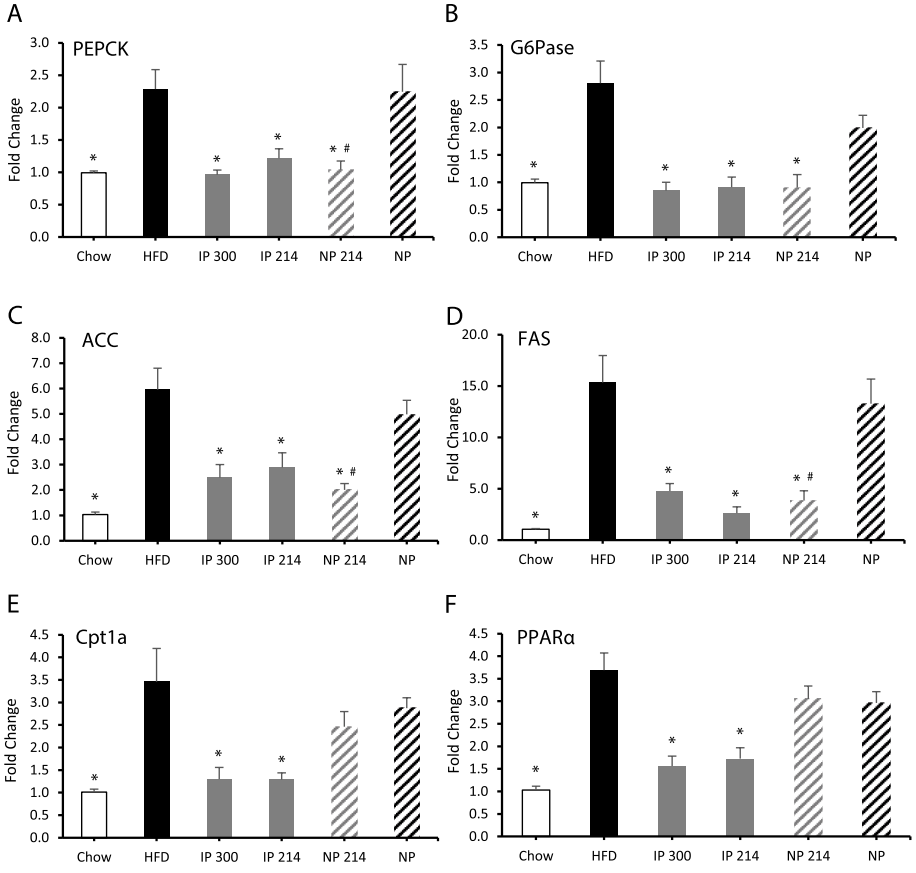

Fig. 4. Effect of PNF treatment in liver gene expression on DIO mouse model. qRT-PCR and relative expression of mRNA transcripts for gluconeogenic genes (A) Phosphoenolpyruvate carboxykinase (PEPCK), (B) Glucose 6-phosphatase (G6Pase). Lipogenic genes, (C) acetyl-CoA carboxylase (ACC), (D) fatty acid synthase (FAS). Catabolism genes, (E) Carnitine Palmitoyltransferase 1a (Cpt1a), and (F) Peroxisome proliferator-activated receptor Alpha (PPARα). Data are expressed as arbitrary units referred to as the level of Cyclophilin B. HFD: High Fat Diet. (n = 4 mice/group). Values were expressed as mean ± standard error. *: $p < 0.05$, all groups vs HFD group. #: $p < 0.05$, NP214 vs NP, ns: non-significant.

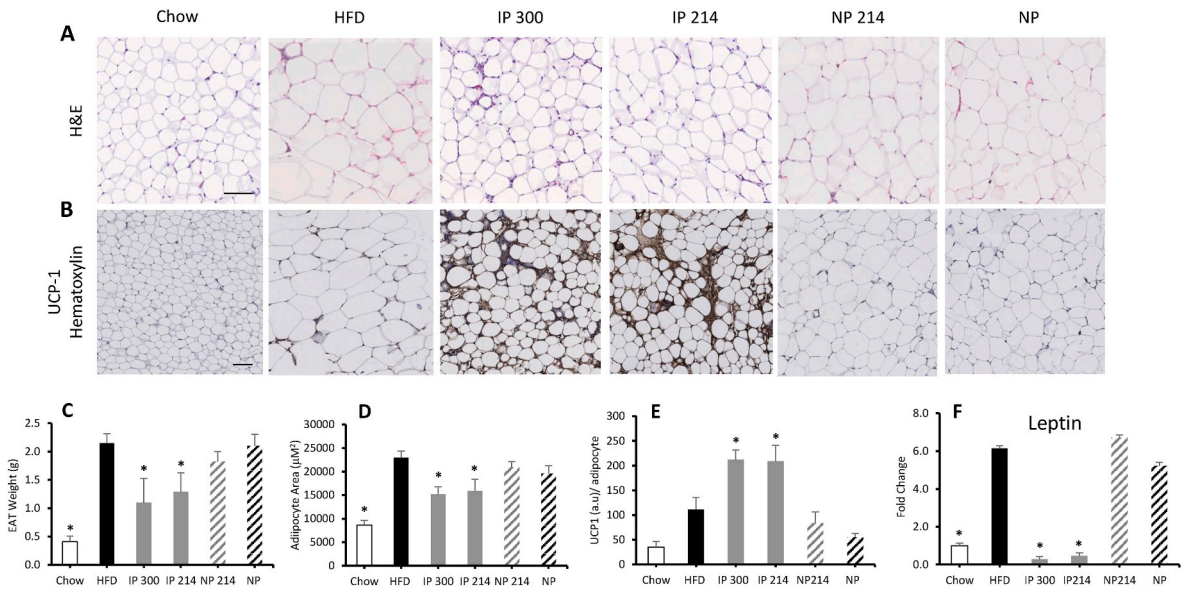

Fig. 5. Effect of PNF treatment on adipocyte tissue in DIO mouse model. (A) Hematoxylin and eosin (H&E) staining of visceral adipose tissue. (B) UCP-1 hematoxylin immunohistological staining. (C) Epididymal adipose tissue (EAT) weight and (D) Adipocyte areas after treatments. (E) Normalized UCP-1 expression and adipocyte area correlation. (F) Relative expression of mRNA transcripts for leptin gene. HFD: High Fat Diet. (n = 4–6 mice/group). Values were expressed as mean ± standard error. *: $p < 0.05$, all groups vs HFD group. #: $p < 0.05$, NP214 vs NP, ns: non-significant. Scale bar = 100 μm.

The emulsion-solvent evaporation method [36] produces NPs with a hydrophobic core to encapsulate compatible OBE100 extract molecules and expose the hydrophilic tails of PLGA on the surface of the NPs to interact with the external hydrophilic medium [37]. The described PLGA NPs presented homogeneous diameters, zeta potential and were suitable for oral administration, as previously reported. The compounds of OBE 100 raw extract are UAL (16%), OA + UA mixture (54%), and an undetermined fraction (UF) (30%) [10,11]. OA and UA were followed as a mixture as being isomers, and they have close retention times and do not allow for following individual peaks (Fig. 1A and Fig. S2). The combination of triterpenes and UF enhanced the beneficial effects in cellular and in-vivo models [14]. On the other hand, OBE100-triterpene proportions produced a larger particle size than empty NPs, which increased as relative viscosity [38] did, in agreement with reports of similar nanoemulsion systems encapsulating hydrophobic compounds [39,40].

PNF is highly efficient in encapsulating 92% of the main components of the crude extract; UAL and OA + UA mixture. The high encapsulation efficiency may be associated with the amphiphilic nature of PLGA [37]. Therefore, UAL of a more hydrophilic nature could be associated with PGA due to its similar polarity, as evidenced by its early peak identified by HPLC. Then, UAL is probably encapsulated in the outer part of the particle [41], showing a greater release extent at pH 3 (40%) and pH 5 (55%) as well as at pH 7 (80%). In contrast, the OA + UA mixture being more hydrophobic, interacted more with the PLA hydrophobic segment of the PLGA polymer at the core of the NPs [42], as evidenced by the late peak from HPLC, thereby showing a lower extent of EE, LC, and release of only up to 40% (Fig. 1F–H).

We preliminarily study the release kinetic profile of OBE100 in a pH 7 PBS solution at 150 rpm and 37 °C to simulate the sink conditions. First, it is essential to note that the release profile of UAL differs from the OA + UA due to their different chemical nature (see Fig. 1F–H and fitting in Table S3). For example, the release kinetics of OA + UA fit better with the Ritger–Peppas and Peppas–Sahlin models when analyzed at 6 and 24 h. It might be related to a coupled mechanism or a superposition of apparently independent Fickian diffusion and polymeric matrix's swelling/relaxation mechanisms. However, K1 and K2 values suggest a higher contribution of Fickian diffusion over polymer matrix relaxation.

When analyzing the cargo release profile on the simulated in-vitro human gastrointestinal conditions (Table S4), the results of UAL and OA + UA fit better with the Peppas-Sahlin models, indicating the complex matrix makes all components release from the NPs with a similar profile [40,41]. In contrast, the release profile of UAL fits better the Lindner-Lippold model that includes the burst [39] related to the release of cargo that is adsorbed at the outermost NP surface or hydration of cargo molecules on the surface. This result is consistent with the more hydrophilic character of UAL that hydrates better than hydrophobic OA + UA, thus UAL presenting a prominent initial burst. Therefore, this fact also supports that the extract molecules are encapsulated in hydrophobic/hydrophilic NPF places, as stated before.

The release results are consistent with the efficient biological activity observed in mice treated with OBE100-loaded NPs (NP214). The significant reduction in body weight, hyperglycemia, hyperinsulinemia, insulin resistance, glucose intolerance, TAG and LDL plasma levels of animals treated with NP214, compared to control animals fed with HFD, is similar in animals with intraperitoneal treatment (Fig. 2, Table 1). Furthermore, the administration of empty NPs does not show a significant difference in most of these parameters, showing that empty NPs do not affect the metabolism of carbohydrates. These results confirm our hypothesis that the developed nanoformulation generates a similar biological effect in reversing the alterations in carbohydrate metabolism that OBE100 intraperitoneally administrated [18]. Additionally, our results indicate that the effect of treatment with NP214 is due to the effect of OBE100 on hepatic lipid metabolism since no weight or fat accumulation reduction is observed in animals treated with empty NPs (Fig. 3B and C).

Encapsulation of *Eucalyptus* sp. *extracts* under different strategies, such as nanocomposites [43], nanogels [44], metallic particles [45–47] and their main fractions, such as UA [48] or OA [49] and eucalyptus essential oil [50], have been reported. Nevertheless, we report the encapsulation of the crude lyophilized extract in PLGA, including UAL, that has not been previously encapsulated. Furthermore, release tests of the enriched-triterpenes extract demonstrated the presence of all its components, including traces of the chemical compounds that have not been identified.

Several studies have shown that oral administration of nanoformulations based on the encapsulation of either single molecules or extracts of natural origin reduces hyperglycemia, hyperlipidemia and

oxidative stress in rat models with type 1 [51,52] or type 2 diabetes [24,53]. Evaluations in obese rats showed that treatments with plant extracts encapsulated in gold NPs reduce body weight and fasting glucose, improving lipid profile, inflammation, and plasma leptin levels [54,55]. These results demonstrate that the administration of these formulations bypasses the liver's metabolic filter and allows biologically active compounds to reach adipose tissue, reducing systemic inflammation and leptin release. In contrast, our work shows that oral nanoformulation did not affect adipose tissue (Table 1, Fig. 5). Biodistribution studies of PLGA reveal that after 21 days of oral administration, the most significant amount of NPs is found in the intestine and liver [56]. It may explain why NP214 treatment affects the liver more than adipose tissue.

The expression and phosphorylation levels of AMPK and ACC were evaluated to explore the possible mechanisms involved in reducing hepatic intracellular fat accumulation. Phosphorylation of ACC produces a drop in the malonyl-CoA levels, inhibiting the synthesis of fatty acids [57]. At the endpoint, the pACC/ACC ratio is similar in all the groups. However, treated groups reduced total ACC expression levels (Fig. 3D and E). It could be hypothesized that the pACC/ACC ratio would be higher during treatment, contributing to increased β-oxidation and reduced intracellular lipid storage. In contrast, empty NPs treatment did not reduce ACC mRNA expression levels (Fig. 4C). Alteration of the protein stability could explain the reduction in the total ACC protein expression by a component of NPs or some nonspecific interaction with an anti-ACC antibody.

Metformin or thiazolidinediones are used to treat insulin resistance and T2DM. AMPK activation has been identified as a mechanism of action [58]. It has been shown that UA activates AMPK, increasing fatty acid oxidation and reducing fat deposition in the liver [59]. AMPK phosphorylates and inactivates ACC, which decreases the synthesis of malonyl CoA and, consequently, increases the oxidation of fatty acids mediated by CPT1α, whose expression is stimulated by PPARα and PGC1 [57]. Intraperitoneal administration of OBE100 reduces the expression of the CPT1α and PPARα genes; however, oral administration of NP214 does not have the same effect (Fig. 4E and F). The interaction between NPs-food in the digestive tract is unknown and may also affect the release and absorption of the OBE100 main components. Our results suggest that the components released and exposed to the liver differ from the proportion of triterpenes identified in the crude fraction of OBE100 and do not affect the expression of CPT1α and PPARα, but they do modulate the expression of other lipogenic and gluconeogenic genes (Fig. 4). Since the administration of empty NPs does not affect the expression of the evaluated genes, the effects identified with NP214 treatment are exclusively due to the action of encapsulated OBE100.

A SHIME model, simulating the basal conditions of the human digestive system, was used to investigate the NP's behaviour (Fig. S1) [60]. In the stomach reactor, NPs release 63% of UAL after 3 h of permanence. The release kinetics in acetate buffer in acidic pH conditions showed 24% UAL release. This difference may be due to the components in the release media and the additional conditions inside the reactor; the presence of additional salts and a more considerable volume could improve the solution's buffer capacity, favoring a better release of the UAL given its more hydrophilic characteristic [61]. The 63% release of UAL is detected at the end of the residence time in the reactor, which disposes it to gastric emptying in the intestine and exposes a more significant amount of the compound for possible absorption. However, it is essential to note that food and plant matrices have a critical role in the bioavailability of triterpenes because they undergo digestion in the mouth, stomach, and duodenum and are subjected to mechanical actions, enzymatic activities, and different pH conditions [15,62].

UAL release is 63% in the stomach and 11% in the small intestine, the cumulative release in these two reactors is 74%. These results are comparable with previous studies of release kinetics in phosphate buffer at pH 7, where the release of this analyte is 76%. The data obtained in the first two reactors increase the availability of the analytes for their possible absorption. On the other hand, the data obtained for the UA + OA mixture show a release of 39 and 29% for the stomach and intestine, respectively, adding a cumulative release of 68%. The detection of this mixture is also more significant in the stomach simulator rector than in the release kinetics at pH3 citrate buffer.

The releases obtained in phosphate buffer at pH 7 are comparable to those obtained in the small intestine reactor, showing that the PNF is consistent in the release process at this pH [63]. The partition coefficients for UA and OA are 6.43 and 6.47, respectively [64], making them poorly soluble. These results show that PNF releases UA + OA mixture up to 91% and UAL up to 82%, improving their solubility and availability to be possibly absorbed in the small intestine. Notably, the lipophilicity of pentacyclic triterpenes strongly influences their interactions with absorbent surface components within the gastrointestinal tract [61].

In conclusion, this study efficiently developed a nanoformulation, encapsulating the OBE100 crude extract and preserving its effects against obesity and T2DM. Administration of the oral nanoformulation improves glucose tolerance, insulin sensitivity, and dyslipidemia and reduces fasting glucose levels in a DIO mouse model. In addition, the mix of bioactive compounds present in OBE100 alters hepatic gene expression and cellular events resulting in the modulation of carbohydrate and lipid metabolism. These results show an alternative for treating obesity and some of its metabolic complications. The idea is to advance the development of drugs based on natural products that can eventually be marketed for their safety and efficacy. Our nanoformulation released up to 91% of the main triterpenes in the extract in an in vitro gastrointestinal model. It opens the way to continue with pre-clinical studies that allow us to assess the nanoformulation's pharmacokinetic, pharmacological, and toxicological parameters.

Author contributions

E.E-C. Writing - original draft, investigation, formal analysis, methodology, visualization. SA DLM, MF, AE, LFE Investigation, formal analysis, validation. JO Conceptualization, formal analyses, Writing - Review & Editing. NB Conceptualization, formal analyses, Writing - Review & Editing, visualization, supervision, project administration, funding acquisition.

Author statement

We appreciate the time and efforts of the editor and referees in reviewing this manuscript. We have addressed all issues indicated in the review report and believe that the revised version could meet the journal publication requirements.

Declaration of competing interest

The authors declare that they have no known competing financial interests or personal relationships that could have appeared to influence the work reported in this paper.

Data availability

No data was used for the research described in the article.

Acknowledgements

This study was supported and funded by Minciencias Colombian grant 111580763027. The authors are grateful to Camila Jimenez and Susana Mejia for their support and assistance in the experiments of PNF. Furthermore, JO acknowledges financial support to Minciencias, the University of Antioquia and the Max Planck Society through the Cooperation Agreement 566-1, 2014. Finally, the authors thank Ruta N and EPM for hosting the tandem groups.

Appendix A. Supplementary data

Supplementary data to this article can be found online at https://doi.org/10.1016/j.jddst.2023.104264.

References

[1] World health organization, Obesity and overweight, Published, 2021, https://www.who.int/news-room/fact-sheets/detail/obesity-and-overweight. (Accessed 10 March 2022).

[2] J.W. Anderson, C.W.C. Kendall, D.J.A. Jenkins, Importance of weight management in type 2 diabetes: review with meta-analysis of clinical studies, J. Am. Coll. Nutr. 22 (5) (2003) 331–339, https://doi.org/10.1080/07315724.2003.10719316.

[3] International Diabetes Federation, IDF Diabetes Atlas, 10TH ed., 2021, https://doi.org/10.1016/j.diabres.2013.10.013.

[4] H. Yanai, Causative anti-diabetic drugs and the underlying clinical factors for hypoglycemia in patients with diabetes, World J. Diabetes 6 (1) (2015) 30, https://doi.org/10.4239/wjd.v6.i1.30.

[5] R.S. Ahima, Digging deeper into obesity, J. Clin. Invest. 121 (6) (2011) 2076–2079, https://doi.org/10.1172/JCI58719.

[6] A.C.M. Munhoz, T.S. Frode, Isolated Compounds from Natural Products with Potential Antidiabetic Activity - A Systematic Review 14 (2017), https://doi.org/10.2174/1573399813666170505120621.

[7] X. Nie, Z. Chen, L. Pang, et al., Oral nano drug delivery systems for the treatment of type 2 diabetes mellitus: an available administration strategy for antidiabetic phytocompounds, Int. J. Nanomed. 15 (2020) 10215–10240, https://doi.org/10.2147/IJN.S285134.

[8] F. Alam, MdA. Islam, M.A. Kamal, S.H. Gan, Updates on managing type 2 diabetes mellitus with natural products: towards antidiabetic drug development, Curr. Med. Chem. 25 (39) (2016) 5395–5431, https://doi.org/10.2174/0929867323666160813222436.

[9] Y.S. Oh, Plant-derived compounds targeting pancreatic beta cells for the treatment of diabetes, Evid. base Compl. Alternative Med. (2015) 1–12, https://doi.org/10.1155/2015/629863. Published online.

[10] A. Guillén, S. Granados, K.E. Rivas, O. Estrada, L.F. Echeverri, N. Balcázar, Antihyperglycemic activity of eucalyptus tereticornis in insulin-resistant cells and a nutritional model of diabetic mice, Adv. Pharmacol. Sci. (2015), https://doi.org/10.1155/2015/418673. Published online.

[11] S. Ceballos, A. Guillén, D.L. Muñoz, et al., Immunometabolic regulation by triterpenes of Eucalyptus tereticornis in adipose tissue cell line models, Phytomedicine 50 (February) (2018) 109–117, https://doi.org/10.1016/j.phymed.2018.03.059.

[12] N. Balcazar, L.I. Betancur, D.L. Muñoz, et al., Ursolic acid lactone obtained from eucalyptus tereticornis increases glucose uptake and reduces inflammatory activity and intracellular neutral fat: an in vitro study, Molecules 26 (8) (2021), https://doi.org/10.3390/molecules26082282.

[13] S. Acín, D.L. Muñoz, A. Guillen, et al., Triterpene-enriched fractions from Eucalyptus tereticornis ameliorate metabolic alterations in a mouse model of diet-induced obesity, J. Ethnopharmacol. (March 2020) (2021) 265, https://doi.org/10.1016/j.jep.2020.113298.

[14] L. Betancur, D. Muñoz, A. Guillen, F. Echeverri, N. Balcazar, S. Acin, Major triterpenoids from Eucalyptus tereticornis have enhanced beneficial effects in cellular models when mixed with minor compounds present in raw extract, *Anais da Academia Brasileira de Ciências*. Published online (2018) 16–23.

[15] N.A.J.C. Furtado, L. Pirson, H. Edelberg, et al., Pentacyclic triterpene bioavailability: an overview of in vitro and in vivo studies, Molecules 22 (3) (2017), https://doi.org/10.3390/molecules22030400.

[16] Q. Jiang, X. Yang, P. Du, H. Zhang, T. Zhang, Dual strategies to improve oral bioavailability of oleanolic acid: enhancing water-solubility, permeability and inhibiting cytochrome P450 isozymes, Eur. J. Pharm. Biopharm. 99 (November) (2016) 65–72, https://doi.org/10.1016/j.ejpb.2015.11.013.

[17] S. Hua, Advances in oral drug delivery for regional targeting in the gastrointestinal tract - influence of physiological, pathophysiological and pharmaceutical factors, Front. Pharmacol. 11 (April) (2020) 1–22, https://doi.org/10.3389/fphar.2020.00524.

[18] A. Sánchez, S.P. Mejía, J. Orozco, Recent advances in polymeric nanoparticle-encapsulated drugs against intracellular infections, Molecules 25 (16) (2020) 1–45, https://doi.org/10.3390/molecules25163760.

[19] H.S. Han, S.Y. Koo, K.Y. Choi, Emerging nanoformulation strategies for phytocompounds and applications from drug delivery to phototherapy to imaging, Bioact. Mater. 14 (October) (2022) 182–205, https://doi.org/10.1016/j.bioactmat.2021.11.027.

[20] T. Vasconcelos, B. Sarmento, P. Costa, Solid dispersions as strategy to improve oral bioavailability of poor water soluble drugs, Drug Discov. Today 12 (23–24) (2007) 1068–1075, https://doi.org/10.1016/j.drudis.2007.09.005.

[21] S. Kalepu, V. Nekkanti, Insoluble drug delivery strategies: review of recent advances and business prospects, Acta Pharm. Sin. B 5 (5) (2015) 442–453, https://doi.org/10.1016/j.apsb.2015.07.003.

[22] K.T. Savjani, A.K. Gajjar, J.K. Savjani, Drug solubility: importance and enhancement techniques, ISRN Pharmaceutics 2012 (100 mL) (2012) 1–10, https://doi.org/10.5402/2012/195727.

[23] J. Wang, J. Tan, J. Luo, et al., Enhancement of scutellarin oral delivery efficacy by vitamin B12-modified amphiphilic chitosan derivatives to treat type II diabetes induced-retinopathy, J. Nanobiotechnol. 15 (1) (2017) 1–17, https://doi.org/10.1186/s12951-017-0251-z.

[24] A. Ahangarpour, A.A. Oroojan, L. Khorsandi, M. Kouchak, M. Badavi, Solid lipid nanoparticles of myricitrin have antioxidant and antidiabetic effects on streptozotocin-nicotinamide-induced diabetic model and myotube cell of male mouse, Oxid. Med. Cell. Longev. 2018 (2018), https://doi.org/10.1155/2018/7496936.

[25] Y. Peng, Q. Meng, J. Zhou, et al., Nanoemulsion delivery system of tea polyphenols enhanced the bioavailability of catechins in rats, Food Chem. 242 (March 2017) (2018) 527–532, https://doi.org/10.1016/j.foodchem.2017.09.094.

[26] M.E. El-Naggar, F. Al-Joufi, M. Anwar, M.F. Attia, M.A. El-Bana, Curcumin-loaded PLA-PEG copolymer nanoparticles for treatment of liver inflammation in streptozotocin-induced diabetic rats, Colloids Surf. B Biointerfaces 177 (February) (2019) 389–398, https://doi.org/10.1016/j.colsurfb.2019.02.024.

[27] M. Prakobvaitayakit, U. Nimmannit, Optimization of polylactic-co-glycolic acid nanoparticles containing itraconazole using 23 factorial design, AAPS PharmSciTech 4 (4) (2003) 1–9, https://doi.org/10.1208/pt040471.

[28] A.B. Shirode, D.J. Bharali, S. Nallanthighal, J.K. Coon, S.A. Mousa, R. Reliene, Nanoencapsulation of pomegranate bioactive compounds for breast cancer chemoprevention, Int. J. Nanomed. 10 (2015) 475–484.

[29] S. D'Souza, A review of in vitro drug release test methods for nano-sized dosage forms, Advances in Pharmaceutics 2014 (2014) 1–12, https://doi.org/10.1155/2014/304757.

[30] A. Polo, C. Cappello, I. Carafa, et al., A novel functional herbal tea containing probiotic Bacillus coagulans GanedenBC30: an in vitro study using the Simulator of the Human Intestinal Microbial Ecosystem (SHIME), J. Funct.Foods 88 (November 2021) (2022) 4–11, https://doi.org/10.1016/j.jff.2021.104873.

[31] A.L. Martínez-López, E. Carvajal-Millan, R. Canett-Romero, et al., Arabinoxylans-based oral insulin delivery system targeting the colon: simulation in a human intestinal microbial Ecosystem and evaluation in diabetic rats, Pharmaceuticals 15 (9) (2022) 1062, https://doi.org/10.3390/ph15091062.

[32] E.L. McConnell, A.W. Basit, S. Murdan, Measurements of rat and mouse gastrointestinal pH, fluid and lymphoid tissue, and implications for in-vivo experiments, J. Pharm. Pharmacol. 60 (1) (2008) 63–70, https://doi.org/10.1211/jpp.60.1.0008.

[33] F. Echeverriá, R. Valenzuela, A. Bustamante, et al., High-fat diet induces mouse liver steatosis with a concomitant decline in energy metabolism: attenuation by eicosapentaenoic acid (EPA) or hydroxytyrosol (HT) supplementation and the additive effects upon EPA and HT co-administration, Food Funct. 10 (9) (2019) 6170–6183, https://doi.org/10.1039/c9fo01373c.

[34] H. Arkaban, M. Barani, M. Akbarizadeh, et al., Polyacrylic acid is a polymer with high permeability due to the carboxylic acid group's greater flexibility, Polymers 14 (1259) (2022) 1–33, https://doi.org/10.3390/polym14061259.

[35] X. He, Y. Zhu, L. Yang, et al., MgFe-LDH nanoparticles: a promising leukemia inhibitory factor replacement for self-renewal and pluripotency maintenance in cultured mouse embryonic stem cells, Adv. Sci. 8 (9) (2021) 11–14, https://doi.org/10.1002/advs.202003535.

[36] M. Iqbal, N. Zafar, H. Fessi, A. Elaissari, Double emulsion solvent evaporation techniques used for drug encapsulation, Int. J. Pharm. 496 (2) (2015) 173–190, https://doi.org/10.1016/j.ijpharm.2015.10.057.

[37] N. Surya, S. Bhattacharyya, PLGA – the smart polymer for drug delivery, Pharmacy. Pharmacol. 9 (5) (2021) 334–345, https://doi.org/10.19163/2307-9266-2021-9-5-334-345.

[38] A. Gupta, H.B. Eral, T.A. Hatton, P.S. Doyle, Nanoemulsions: formation, properties and applications, Soft Matter 12 (11) (2016) 2826–2841, https://doi.org/10.1039/c5sm02958a.

[39] Z. Goktas, Y. Zu, M. Abbasi, et al., Recent advances in nanoencapsulation of phytochemicals to combat obesity and its comorbidities, J. Agric. Food Chem. 68 (31) (2020) 8119–8131, https://doi.org/10.1021/acs.jafc.0c00131.

[40] S.P. Mejía, A. Sánchez, V. Vásquez, J. Orozco, Functional nanocarriers for delivering itraconazole against fungal intracellular infections, Front. Pharmacol. (2021;12(June) 1–16, https://doi.org/10.3389/fphar.2021.685391.

[41] W. Wang, W. Zhang, Y. Jiang, et al., Preparation of ursolic acid–phospholipid complex by solvent-assisted grinding method to improve dissolution and oral bioavailability, Pharmaceut. Dev. Technol. 25 (1) (2020) 68–75, https://doi.org/10.1080/10837450.2019.1671864.

[42] C. Wischke, S.P. Schwendeman, Principles of encapsulating hydrophobic drugs in PLA/PLGA microparticles, Int. J. Pharm. 364 (2) (2008) 298–327, https://doi.org/10.1016/j.ijpharm.2008.04.042.

[43] C.G. Silva, P.A.L. Campini, D.B. Rocha, D.S. Rosa, The influence of treated eucalyptus microfibers on the properties of PLA biocomposites, Compos. Sci. Technol. 179 (January) (2019) 54–62, https://doi.org/10.1016/j.compscitech.2019.04.010.

[44] P. Sahu, S.K. Kashaw, S. Jain, S. Sau, A.K. Iyer, Assessment of penetration potential of pH responsive double walled biodegradable nanogels coated with eucalyptus oil for the controlled delivery of 5-fluorouracil: in vitro and ex vivo studies, J. Contr. Release 253 (2017) 122–136, https://doi.org/10.1016/j.jconrel.2017.03.023.

[45] P. Salgado, D.O. Mártire, G. Vidal, Eucalyptus extracts-mediated synthesis of metallic and metal oxide nanoparticles: current status and perspectives, Mater. Res. Express 6 (8) (2019), https://doi.org/10.1088/2053-1591/ab254c.

[46] M. Balamurugan, S. Saravanan, T. Soga, Synthesis of iron oxide nanoparticles by using eucalyptus globulus plant extract, e-J. Surf. Sci. Nanotechnol. (2014;12 (August) 363–367, https://doi.org/10.1380/ejssnt.2014.363.

[47] H. Sawalha, R. Abiri, R. Sanusi, et al., Toward a better understanding of metal nanoparticles, a novel strategy from eucalyptus plants, Plants 10 (5) (2021) 1–22, https://doi.org/10.3390/plants10050929.

[48] L. Wang, Q. Yin, C. Liu, Y. Tang, C. Sun, J. Zhuang, Nanoformulations of ursolic acid: a modern natural anticancer molecule, Front. Pharmacol. (2021;12(July), https://doi.org/10.3389/fphar.2021.706121.
[49] M. Chen, Z. Zhong, W. Tan, S. Wang, Y. Wang, Recent advances in nanoparticle formulation of oleanolic acid, Chin. Med. 6 (2011) 2–5, https://doi.org/10.1186/1749-8546-6-20.
[50] C.S. Vali, A. Khan, M.P. Bharathi, S.S. Prasad, A. Srikanth, Development and characterization of Eucalyptus oil loaded poly lactic Co-glycolic acid - albumin nanocapsules, Int. J. Pharmaceut. Sci. Rev. Res. 68 (1) (2021) 206–212, https://doi.org/10.47583/ijpsrr.2021.v68i01.032.
[51] S. Amjadi, M. Mesgari Abbasi, B. Shokouhi, M. Ghorbani, H. Hamishehkar, Enhancement of therapeutic efficacy of betanin for diabetes treatment by liposomal nanocarriers, J. Funct.Foods (2019;59(May) 119–128, https://doi.org/10.1016/j.jff.2019.05.015.
[52] R. Rani, S. Dahiya, D. Dhingra, N. Dilbaghi, K.H. Kim, S. Kumar, Improvement of antihyperglycemic activity of nano-thymoquinone in rat model of type-2 diabetes, Chem. Biol. Interact. 295 (2018) 119–132, https://doi.org/10.1016/j.cbi.2018.02.006.
[53] Y. Zhang, J. Li, Z. Wang, et al., Natural plant-derived polygalacturonic acid-oleanolic acid assemblies as oral-delivered nanomedicine for insulin resistance treatment, Chem. Eng. J. 390 (January) (2020), 124630, https://doi.org/10.1016/j.cej.2020.124630.
[54] L. Gao, Y. Hu, D. Hu, et al., Anti-obesity activity of gold nanoparticles synthesized from Salacia chinensis modulates the biochemical alterations in high-fat diet-induced obese rat model via AMPK signaling pathway, Arab. J. Chem. 13 (8) (2020) 6589–6597, https://doi.org/10.1016/j.arabjc.2020.06.015.
[55] S.A. Ansari, A. Bari, R. Ullah, M. Mathanmohun, V.P. Veeraraghavan, Z. Sun, Gold nanoparticles synthesized with Smilax glabra rhizome modulates the anti-obesity parameters in high-fat diet and streptozotocin induced obese diabetes rat model, J. Photochem. Photobiol. B Biol. 201 (2019), 111643, https://doi.org/10.1016/j.jphotobiol.2019.111643.
[56] S.M. Navarro, T.W. Morgan, C.E. Astete, et al., Biodistribution and toxicity of orally administered poly (lactic-co-glycolic) acid nanoparticles to F344 rats for 21 days, Nanomedicine 11 (13) (2016) 1653–1669, https://doi.org/10.2217/nnm-2016-0022.
[57] S. Song, R.R. Attia, S. Connaughton, et al., Peroxisome proliferator activated receptor α (PPARα) and PPAR gamma coactivator (PGC-1α) induce carnitine palmitoyltransferase IA (CPT-1A) via independent gene elements, Mol. Cell. Endocrinol. 325 (1–2) (2010) 54–63, https://doi.org/10.1016/j.mce.2010.05.019. Peroxisome.
[58] M. López, R. Nogueiras, M. Tena-Sempere, C. Diéguez, Hypothalamic AMPK: a canonical regulator of whole-body energy balance, Nat. Rev. Endocrinol. 12 (7) (2016) 421–432, https://doi.org/10.1038/nrendo.2016.67.
[59] S. Herzig, R.J. Shaw, AMPK: guardian of metabolism and mitochondrial homeostasis Sébastien, Nat. Rev. Mol. Cell Biol. 19 (2) (2018) 121–135, https://doi.org/10.1038/nrm.2017.95.AMPK.
[60] T Van de Wiele, P Van den Abbeele, W. Ossieur, S. Possemiers, M. Marzorati, The simulator of the human intestinal microbial Ecosystem (SHIME ®), in: K. Verhoeckx, P. Cotter, I. López-Expósito, et al. (Eds.), The Impact of Food Bioactives on Health: in Vitro and Ex Vivo Models, First edit. Springer International Publishing, 2015, pp. 1–327, https://doi.org/10.1007/978-3-319-16104-4.
[61] S. Fredenberg, M. Wahlgren, M. Reslow, A. Axelsson, The mechanisms of drug release in poly(lactic-co-glycolic acid)-based drug delivery systems - a review, Int. J. Pharm. 415 (1–2) (2011) 34–52, https://doi.org/10.1016/j.ijpharm.2011.05.049.
[62] M.J. Rein, M. Renouf, C. Cruz-Hernandez, L. Actis-Goretta, S.K. Thakkar, M. da Silva Pinto, Bioavailability of bioactive food compounds: a challenging journey to bioefficacy, Br. J. Clin. Pharmacol. 75 (3) (2013) 588–602, https://doi.org/10.1111/j.1365-2125.2012.04425.x.
[63] P. Artursson, K. Palm, K. Luthman, Caco-2 monolayers in experimental and theoretical predictions of drug transport, Adv. Drug Deliv. Rev. 64 (SUPPL) (2012) 280–289, https://doi.org/10.1016/j.addr.2012.09.005.
[64] C. Bérangère, N. Caussarieu, P. Morin, L. Morin-Allory, M. Lafosse, Rapid analysis of triterpenic acids by liquid chromatography using porous graphitic carbon and evaporative light scattering detection, J. Separ. Sci. 27 (12) (2004) 964–970, https://doi.org/10.1002/jssc.200401764.